# Negatively Competitive Incoherent Feedforward Loops Mitigate Winner-Take-All Resource Competition

Austin Stone<sup>1</sup>, Jordan Ryan<sup>2</sup>, Xun Tang<sup>2</sup>, Xiao-Jun Tian\*,<sup>1</sup>

#### **ABSTRACT**

The effects of host resource limitations on the function of synthetic gene circuits have gained significant attention over the past years. Hosts, having evolved resource capacities optimal for their own genome, have been repeatedly demonstrated to suffer from the added burden of synthetic genetic programs, which may in return pose deleterious effects on the circuit's function. Three resource controller archetypes have been proposed previously to mitigate resource distribution problems in dynamic circuits: the local controller, the global controller, and a "negatively competitive" regulatory (NCR) controller that utilizes synthetic competition to combat resource competition. The dynamics of negative feedback forms of these controllers have been previously investigated, and here we extend the analysis of these resource allocation strategies to the incoherent feedforward loop (iFFL) topology. We demonstrate that the three iFFL controllers can attenuate Winner-Take-All resource competition between two bistable switches. We uncover that the parameters associated with the synthetic competition in the NCR iFFL controller are paramount to its increased efficacy over the local controller type, while the global controllers demonstrate to be relatively ineffectual. Interestingly, unlike the negative feedback counterpart topologies, iFFL controllers exhibit a unique coupling of switch activation thresholds which we term the "coactivation threshold shift" (CTS) effect. Finally, we demonstrate that a nearly fully orthogonal set of bistable switches could be achieved by pairing an NCR controller with an appropriate level of controller resource consumption.

**Keywords**: modularity, resource competition mitigation, gene networks, sensitivity analysis, orthogonality

<sup>&</sup>lt;sup>1</sup> School of Biological and Health Systems Engineering, Arizona State University, Tempe, AZ 85281, United States.

<sup>&</sup>lt;sup>2</sup> Cain Department of Chemical Engineering, Louisiana State University, Baton Rouge, LA 70803, United States.

<sup>\*</sup>Corresponding Author E-mail: xiaojun.tian@asu.edu

#### INTRODUCTION

Modularity is an important tenet which the forward-engineering process is built upon; component modularity and orthogonality to context allow components to behave in a predictable and robust manner across a broad range of circuit configurations and environments. Although synthetic biosystems engineering has reached maturity over the past decade as an engineering discipline via application of traditional design principles to biological constructs, development of circuits is still hindered in large part by modes of context-dependence and nonmodularity unique to biological systems<sup>1-5</sup>. One important and universal origin of component nonmodularity in gene circuits is the competition over limited pools of transcriptional and translational resources (RNAP and ribosomal components respectively)<sup>6-9</sup>. Traditional gene circuit models often assume unlimited resources for simplification; however, in realistic systems, genes that have been designed to be completely orthogonal to each other will consistently demonstrate indirect repressive crosslinks due to the dip in transcriptional/translational resources available to one caused by increased expression in the other. The unintended repressive links caused by limited resources not only cause the circuit behavior to deviate from predictions of mathematical models but also may result in a complete collapse of function in circuits with nontrivial dynamics. A notable example is the "Winner-Take-All (WTA)" phenomenon, whereby activation of a bistable switch turns a purportedly orthogonal second bistable switch off by stealing transcriptional/translational resources<sup>10</sup>. Resource competition has also been indicated to increase noise coupling between genes and potentially increase gene expression noise in multigene systems<sup>11</sup>.

To handle the deleterious effects of resource competition, numerous control strategies have been proposed in the past. Utilizing orthogonal resource pools (orthogonal ribosomes/RNAP systems) has shown decent efficacy in insulating different subsystems from fighting over shared resources<sup>12,13</sup>, while splitting circuit subsystems across multi-strain consortia has been demonstrated to split expression burden across a population in a manner that alleviates resource competitive effects<sup>10,12–15</sup>. We previously investigated three topologically different negative feedback controllers, the global, local, and our own proposed "negatively competitive" regulatory (NCR) controller architectures from a systems control standpoint<sup>16</sup>. The NCR controller utilizes competition to fight against the competition, wherein repressive sgRNAs expressed by circuit modules were forced to compete over a limited pool of CRISPR moiety to instigate repression. Global controllers (GC) and local controllers (LC), on the other hand, mediate regulation via simple circuit-wide and module-specific levels of control, respectively.

These control strategies utilize common network motifs to regulate intracellular resource distribution in a manner much like cells in nature do, rather than resorting to the implementation of exogenous biochemical machinery or consortia engineering, and have been utilized extensively by synthetic biosystems engineers as resource allocation controllers in the past <sup>17–20</sup>. Our previous investigations demonstrated that the inflexible architecture of the global negative feedback controller results in limited efficacy in fighting against WTA resource competition and resource competitive noise, while the flexible architecture and dual effect of our proposed NCR controller resulted in strong repression of WTA resource competition <sup>16</sup> and resource competitive noise<sup>11</sup>.

Incoherent feedforward loops (iFFLs) couple both activation and repression arms and have been implicated to function in adaptation behavior and pulse generation<sup>21–24</sup>. They have also been demonstrated to function as resource regulators<sup>25-28</sup> due to the repressive links inherent to the iFFL architecture, much like the negative feedback motif. Here we extend our analysis of the aforementioned three controller architectures to iFFLs. Specifically, we study the effects of these controllers by applying them to the dual self-activation (DSA) circuit, a model circuit for studying resource competition comprised of two inducible, bistable self-activation switches which are unlinked other than the resource competition between them. We utilize steady-state heatmap analysis in silico to demonstrate that the global, local, and NCR iFFLbased controllers tend to follow a similar pattern as the negative feedback controllers in fighting against WTA resource competition, with NCR and local controllers successfully attenuating resource competitive phenomena and the global controllers demonstrating limited efficacy. Global and local parameter sensitivity analysis unveils that the level of competition of sgRNAs over the dCas9 moiety and system symmetry are critical to NCR's ability to outperform the local controller. Unexpectedly, we find that the contralateral links between modules lead to a notable shifting of coactivation thresholds that is a unique aspect of iFFL-typed controllers, which we coin the "coactivation threshold shift" phenomenon. Lastly, we demonstrate that NCR systems tend to result in a unique negative coactivation threshold shift which, when combined with resource consumption of the controller nodes, can result in almost perfect module insulation from context-dependent resource competition even in the presence of limited resources.

#### **RESULTS**

WTA resource competition in dual self-activation circuit and iFFL controller topologies

Figure 1 demonstrates the effect of resource competition on the dual-self activation (DSA) circuit (Figure 1A). The DSA circuit comprises two orthogonal bistable self-activation switches, with each switch taking an inducer (I1 or I2 respectively). This differs from the original cascading bistable switch circuit in Zhang et al. 10 by the removal of the direct connections between the two modules. In this fashion, the DSA circuit is much easier to probe for resource competition behavior than the original cascading bistable switch. Given the lack of direct connections between each switch module, any relationship between their activities can be solely attributed to resource competitive effects. In the context of limited resources, competition over resources results in unintended repressive crosslinks (red dashed lines) between the two modules, attenuating the extent to which the modules are mutually orthogonal. The effect of these indirect inhibitions can be best assessed in terms of the coactivation region of the switches in the inducer I1-I2 phase space. In the absence of resource competition (Figure 1B), the activation thresholds remain independent of the contralateral inducer, resulting in 4 basins: a no activation basin (white), a Switch 1 activation basin (magenta), a Switch 2 activation basin (blue), and a large coactivation basin (green). However, when the cellular resource is limited, competition over resources would compromise the system's capability of sustaining both switches in the activated state, as indicated by the shrunken coactivation basin in Figure 1C. Much of the coactivation basin is replaced with the new WTA regions, where the switch with a higher activity will win over the resources and force the switch with a lower activity to the off state. Therefore, attenuation of the WTA phenomenon requires re-expansion of this coactivation region.

Three types of negative feedback controllers, including global, local and NCR controllers, have been investigated in our previous work <sup>16</sup>. Here, we will here focus on the incoherent feedforward forms of these controllers. The three types of iFFL controllers are shown in Figure 1D. Each module of the iFFL systems is composed of two nodes: a circuit node (in the DSA case, a self-activation switch) and a controller node that takes the same inducer input as the circuit node it is regulating and directly inhibits the circuit node. For the global controller archetype, all controller nodes generate a universal output that can repress all the genes in the circuit. In other words, the global controller can be considered as one node that sums all the inputs to the circuit and generates circuit-wide repression as a response. Barajas et al. utilized a similar global architecture of circuit-wide activation (rather than repression) by coexpressing the hydrolysis domain of SpoTH to upregulate free ribosome production with the gene of interest, resulting in sufficient resources to overcome the increased resource load of the gene of interest <sup>27</sup>. In the local controller archetype, on the other hand, each controller node represses only the gene it is regulating. Jones et al. also demonstrated the efficacy of this controller type by

coexpressing an endoribonuclease along with the gene-of-interest, which targets the mRNA of gene-of-interest, thereby mitigating the resource consumption of the gene-of-interest via a local feedforward control mechanism <sup>28</sup>. Lastly, the NCR controller is a combination of the two archetypes by utilizing inhibitory CRISPR moieties (CRISPRi) with each controller node only generating the sgRNAs that are repressive to the gene they are controlling. C1 and C2, in this case, diagrammatically represent the production of sgRNA that is repressive against switch 1 and switch 2, respectively, but these can only effectively mediate repression after combining with a dCas9 moiety. However, these sgRNAs will compete over a limited pool of dCas9, and consequently, the NCR controller has both local and global-like attributes. With NCR, the overactive modules not only increase their own repression via the repressive feedforward arms, they also contralaterally activate the less active modules by pulling CRISPR-moiety away from these modules. This form of competitive control is unique to the NCR controller.

#### Mitigation of WTA resource competition by iFFL controllers

Figures 2A-C demonstrate the steady state behavior of the DSA system in the presence of resource competition with the local, global, and NCR iFFL controllers applied, respectively. Although all the controllers re-expand the coactivation basin compared to the baseline resource-competitive case, the global controller performs poorly while the local and NCR controllers demonstrate efficacy in restoring the coactivation region and mitigating the size of the WTA regions. As shown in Figure 2D, as the controller strength increases, the capability of the local and the NCR controllers in reducing the WTA effects and restoring the coactivation basin becomes more significant, within biologically feasible parameter ranges. Here, 'RC' refers to the scenario with resource competition and 'no RC' refers to the scenario without controller or resource competition. Thus, the iFFL-based local and NCR controllers are effective in reducing resource competitive phenomena.

To study the robustness of these controller behaviors over a broad range of relevant biological parameters, we performed global parameter sensitivity analysis utilizing Latin-Hypercube Sampling (detailed further in Methods) on the resource competitive and controller parameters:  $Q_{mij}$  (RNAP-activated promoter binding constant),  $Q_{bmij}$  (base RNAP-promoter binding constant),  $Q_{pij}$  (ribosome-RBS binding constant),  $Q_{xi}$  (controller moiety-promoter binding constant),  $Q_{xi}$  (sgRNA-dCas9 binding constant), and  $Q_{c}$  (dCas9 concentration for NCR controller, multiplier of repressive moiety-promoter binding affinity in the local and global controllers). With our nominal parameter set (Table S1), global sensitivity analysis shows that the performance of NCR controller in restoring the coactivation region is similar to the local controller, while both the NCR

and the local controllers outperform global controllers by a significant margin (Figure 2E). Here, 'RC' refers to the scenario with resource competition but no controller applied. Interestingly, further local parameter sensitivity analysis unveils that the parameter associated with CRISPRmediated competition (biochemically, the dissociation constant between sgRNAs and the CRISPR moiety), J, strongly dictates this relationship. As shown in Figure 2F, increasing the value of J (i.e., decreasing sgRNA binding affinity) decreases the ratio of the coactivation fractions between NCR and the local controllers in a relatively linear fashion approaching 1 for higher J values. This phenomenon is understandable from a biochemical point of view since the NCR controller draws its advantage from introducing the competition of sgRNAs over dCas9 into the system to offset resource competition. As J increases, the binding affinity between the sgRNAs and dCas9 falls, resulting in an increased concentration of free dCas9 and consequently reduced competition over the dCas9 moieties. The synthetic competition in the NCR controller virtually disappears for very large values of J. At this point, the NCR controller resembles the local controller topologically as each circuit module experiences repression from itself solely. This is one of the reasons that the NCR iFFL controller rarely underperforms when compared to the local controller in the global parameter sensitivity analysis over a broad range of relevant biological parameters.

One difference between the global and local sensitivity analysis in Figure 2E-F was that a symmetric system was used in the latter, where parameters for each switch module were set to be equivalent, and J1 always equals J2. As the local sensitivity analysis in Figure 2F demonstrates a notable advantage of NCR controllers over local controllers, we hypothesized that system symmetry also plays a role in distinguishing efficacy between the NCR and local controllers. Figure 2G demonstrates global sensitivity analysis performed with a symmetry constraint applied (parameters for each of the two switch modules were constrained to always be equivalent) and demonstrates that the efficacy of the NCR controller begins to outpace that of the local controller for symmetrical systems with lower J. Furthermore, the distributions and averages of the ratio between the coactivation fraction of the NCR and local controllers are shown in Figures S1-S2 for different global sensitivity analysis runs with different settings for J and symmetry constraints. Lower ranges of J and increasing system symmetry constraints result in an increasingly rightward shifted distribution for the NCR vs LC efficacy ratio above 1.

To demonstrate the effects of controller strength asymmetry, we calculated controller coactivation fraction across various J1 and J2 values, and the corresponding heatmaps in Figures 2H-J confirm that each controller responds differently to controller strength asymmetry.

Specifically, the local controller is relatively agnostic to asymmetry, and the global controller performs better as the controller strengths become more asymmetric. On the other hand, the NCR controller demonstrates superb performance for symmetrical strengths but performs poorly for asymmetrical controller strengths. These observations explain that, although local and NCR controllers perform similarly on average, controller (a)symmetry strongly dictates when one may outperform the other.

## Unique Coactivation Threshold Shift Phenomenon Differentiates the Three iFFL Controller types

One notable effect found in global and the NCR iFFL controllers but not in the local controller is a shift of the dual-activation point (red circle in Figure 3A) that separates the no-activation basin from the coactivation basin. Here we quantify this "coactivation threshold shift" (CTS) effect by the directional distance from the normalized point (1,1) where the dual activation point is expected to be to the actual dual activation point (Figure 3A). This CTS effect is due to the presence of nontrivial controller-mediated repression/activation of the contralateral circuit node upon induction of either of the nodes even prior to switch activation. This effect is unique to the iFFL controllers and has not been noted previously in the negative feedback controllers<sup>16</sup>, in which the activity of the controller is strictly linked to the circuit node activity. That is, the controller activity in negative feedback controllers is minimal when the switches have not yet been activated. However, this is not true in the iFFL case, as the circuit and the controller nodes are separate. Stimulation with one inducer will cause the respective controller activity to rise and consequently repress/activate the contralateral circuit node, even while the circuit nodes remain inactive.

Notably, the CTS effect manifests differently for the three controller archetypes. Figure 3B demonstrates the CTS magnitudes gathered from the controller heatmaps in Figures 2A-C and the ideal and no controller heatmaps in Figures 1B&C. As the global controller punishes all circuit nodes for the activity of one (Figure 3C), this repressive interdependence results in the activation thresholds of each non-stimulated switch rising, causing the dual-activation point to shift above the (1,1) position and "positive" CTS effect with a positive distance value. Positive CTS results expansion of the no-activation region into the WTA and single-switch-activation regions (Figure 2B). Notably, pushing the dual-activation point outwards could recede the coactivation region even further. This effect alone makes the iFFL global controller significantly worse than the other two archetypes and also worse than the negative feedback global controller for which the coactivation threshold shift effect is not present. This effect is

responsible for the diminishing coactivation fraction of global controllers after a certain point in Figure 2D as the loss of coactivation space from the positive CTS begins to undo the expansion benefits global controllers provide. On the other hand, the negatively competitive nature of the NCR controller results in dCas9 getting pulled away from other switches when one switch is activated. Consequently, the NCR controller creates an activatory correlation between nodes (Figure 3C) and causes the activation thresholds of other circuit switches to fall with increased stimulation of one switch, thus shifting the dual-activation point under the (1,1) position, leading to a "negative" CTS effect with a negative distance value. In other words, unlike the other controller archetypes, two layers of incoherent feedforward loop exist in NCR controllers: the explicit one from the inducer to its module using one direct activating link and one repressive link via controller node (I2->M2 and I2→C2--|M2), and another implicit one from inducer to the opposite module using an activating link through its control node and one inhibitive link via its module (I2->C2->M1 and I2→M2--|M1). This unique structure of the NCR controller results in its unique negative CTS effect. Negative CTS results in contraction of the no-activation region as the single-switch-activation regions begin to infringe on the (1,1) box. Finally, since each local controller node only affects the circuit node it regulates, the local controller demonstrates little to no CTS effects. This trend in CTS across the controller types remains the same as controller strength is increased, but the magnitude of CTS in the global and NCR controllers increases with increasing controller strength (Figure 3D). The global sensitivity analysis in Figure 3E confirms the distinct positive, negative, and neutral CTS effects of the global, NCR, and local controllers, respectively, across the biologically relevant parameter ranges.

### Effect of Controller Resource Consumption and Construction of a Nearly Orthogonal Switch System

Up to here, only resource consumption by the circuit nodes has been taken into account while resource consumption by the controller itself has been assumed to be negligible. This is a valid assumption if the controller is mediated via sgRNA or small molecule production as the time required for RNAP or ribosome to be bound to transcripts involved in the production of these moieties is significantly smaller than the transcription/ translation of factors/reporters in circuit. However, for controllers mediated via the production of larger transcripts or proteins, controller nodes will consume considerable levels of transcriptional/translational resources and may result in stronger WTA effects if the consumed resources by them outweigh their desired regulatory effects.

To investigate the effect of nontrivial resource consumption by the controller, the controller resource competition (CRC) parameter was introduced into our model. Figure 4A shows the CTS magnitude as the CRC increases. In all three archetypes, the controller resource competition gives rise to a positive CTS effect. Biochemically, adding controller resource consumption creates repressive cross-correlations between the switches through resource competition as shown in Figure 4B. The no-controller case still demonstrates increasing positive CTS as controller resource consumption increases. The reason is that our model still includes the controller nodes without any control ability in the no-controller case for a fair comparison. Consequently, increasing their resource consumption will still reduce the effective resource pool allotted to the circuit nodes, resulting in increasing positive CTS with increasing CRC even though the controller nodes are disconnected from the circuit. As one switch is stimulated, the controller for the activated module will pull resources away from the contralateral switch, and result in an increased activation threshold of the contralateral switch. Notably, this effect stacks with other CTS effects. If controller resource consumption is significant enough, the added positive CTS can offset the negative shift caused by the NCR controller. In contrast, controller resource consumption causes the positive CTS of the global controller to increase the shift further, and makes the local controller shift from neutral to positive.

Previously we demonstrated that the NCR iFFL controller is highly efficacious at increasing the coactivation basin of the dual self-activation switch circuit, and due to its negative CTS effect, it can even increase the coactivation basin to a size larger than the ideal system without resource competition, by pulling the dual activation point under the (1,1) position. Although a larger coactivation fraction may be desirable, the NCR controller's negative CTS at high strength increases coactivation fraction at the expense of orthogonality. Since controller resource consumption is a consistent way to add a positive shift, we hypothesized that we could increase the orthogonality of the NCR controller by adding mild levels of controller resource consumption to offset NCR's negative CTS, while keeping the large coactivation basin provided by NCR's resource regulatory capabilities.

In order to study the effects on orthogonality, we defined an orthogonality score OrthoScore (see details in the methods), which is at a maximum of 1 in a perfectly orthogonal system. As shown in Figure 4C, as *CRC* increases from zero, the OrthoScore of the NCR system rises to a maximum at *CRC*=0.44, where the positive CTS from the controller resource consumption counterbalances the negative shift from NCR, before it begins to decrease as the CTS effect from *CRC* becomes dominant and begins shifting the dual-activation point above the (1,1)

position. On the other hand, the coactivation fraction decreases steadily as *CRC* increases. Consequently, the addition of *CRC* increases the orthogonality of the switches by decreasing and restoring the coactivation basin to the proper dimensions given by the ideal case without resource competition. Figures 4D & 4E compare the heatmaps of the NCR system with no controller resource consumption and the level of *CRC* that maximizes switch orthogonality. As can be clearly seen, the system with an optimized level of controller resource consumption matches the ideal system without resource competition much more closely, with inter-basin boundaries straighter and less dependent on the contralateral inducer.

#### **DISCUSSION**

Competition over limited cellular resources creates unintended crosslinks between modules of synthetic gene circuits. As all organisms and cells utilize limited pools of RNA polymerases and ribosomes, the effects of resource limitation/competition can be seen widely across synthetic biology. When paired with dynamic circuits, the effects of competition can often yield nonintuitive and unintended consequences which hamper forward-engineered design. In addition to local and global feedback topologies, we previously posited a novel resource allocation controller to combat the problem associated with resource competition, which we coined a "negatively competitive regulatory" topology. Unlike the other modes of regulation, the function of the NCR topology can best be viewed as tackling resource consumption of an overactive module via a two-pronged approach: both increasing repression against the overactive module via increased dCas9 targeting and removal of repression on the lower-active modules as the increased targeting of dCas9 towards the overactive module reduces the free dCas9 left to repress the rest of the circuit.

In our previous work,<sup>16</sup> we investigated the local, global, and NCR resource allocation strategies mediated via negative feedback instead of the incoherent feedforward network motif. One notable difference we find here between the negative feedback and the iFFL-mediated resource allocators is the lack of a significant CTS effect in the negative feedback controllers. This is because, in the negative feedback constructs we explored, controller activity was strictly linked to the circuit activity as circuit nodes acted for controller nodes (circuit nodes mediated their own self-repression). As a result, the controller activity is minimal under the switch activation thresholds, preventing any effects on the contralateral switches under the threshold. As resource controller consumption consistently adds positive CTS to DSA systems regardless of controller type, the lack of any negative CTS in the negative feedback NCR controllers removes the buffer that the iFFL NCR controllers have against controller resource consumption. On the

other hand, the global controller may perform better when mediated via negative feedback instead of iFFLs, as the significant positive CTS present in the global iFFL controllers can not only prevent any re-expansion of the coactivation region granted by the controller but may also significantly worsen the orthogonality when compared to a system with resource competition alone.

One important point we demonstrate about the three iFFL controllers is that each has a unique response to system asymmetry. The NCR controller works well for symmetric systems, the global controller works well for asymmetric systems, and the local controller seems to be relatively agnostic to system asymmetry. This stark difference in response between the NCR and global controllers is understandable biochemically. The circuit-wide architecture of the global controller distributes repression relatively evenly across circuit modules. Consequently, any asymmetries in the system are not accentuated by the action of the global controller. The action of the NCR controller, on the other hand, accentuates differences in controller strength. If one arm of the NCR controller is weaker than the others, not only does it mediate less self-repression on the module it directly regulates, but it also poorly activates opposing modules.

Here we demonstrate that the fundamental principles these controller types are built from can be extrapolated generally to a number of motifs, specifically, the incoherent feedforward loop motif. Via steady-state and parameter sensitivity analysis, we demonstrate that the NCR and the local iFFL controller topologies are more efficacious in reversing the effects of resource competition and restoring the DSA circuit functionality than the global archetypes within the biologically relevant parameter ranges. NCR demonstrates a strong advantage over the local controller in cases where the controller strength is symmetric across controller modules (similar values of J), while the local controller outperforms NCR for highly asymmetric systems. That is, when we design the controller, we need to tune the controller strength for each module to achieve optimal control. We showed that different contralateral effects of controller topologies result in different forms of coactivation threshold shift (positive, negative, neutral). Lastly, we demonstrated that the negative coactivation threshold shift effect of the NCR controller could be paired with the positive coactivation threshold shift guaranteed by controller resource consumption to keep controller-mediated reduction of resource competitive effects while negating coactivation threshold shift, creating a set of nearly orthogonal switches even in the presence of resource competition.

#### **METHODS**

To model the dynamics of the different iFFL controllers, we built a mathematical model utilizing a system of ordinary differential equations (ODEs). Specifically, we model the output levels of the mRNA  $M_{ij}$  and the protein  $P_{ij}$ , of both the circuit and the controller nodes as following,

$$\frac{d[M_{ij}]}{dt} = CN * v_{mij} \frac{1/Q_{bmij} + {R_{ij}}/Q_{mij}}{PFm} - d_{mij}[M_{ij}]$$

$$\frac{d[P_{ij}]}{dt} = v_{pij} \frac{{M_{ij}}/Q_{pij}}{PFp} - d_{pij}[M_{ij}]$$

where CN represents gene copy number,  $v_{mij}$  and  $v_{pij}$  represent the per copy transcription and translation rates, respectively.  $Q_{bmij}$  and  $Q_{mij}$  represent the Michaelis-Menten constant for transcriptional for the base and the activated promoter, respectively.  $Q_{pij}$  represents the Michaelis-Menten constant for translational sensitivity,  $d_{mij}$  and  $d_{pij}$  represent the degradation rates of mRNA and protein, respectively, and  $R_{ij}$  represents the fraction of active ij-th promoter. The i index denotes which circuit module is being modeled (for the DSA circuit, i runs from 1 to 2) while the j index denotes whether the circuit node (j = A) or the controller node (j = B) is being modeled. This system of subscripts is illustrated in Figure S3. The PFm and PFp terms model the repression due to competition over RNAPs and ribosomes, respectively:

$$PFm = 1 + \lambda_{RC}CN \sum_{i} \sum_{j} \left( \frac{1}{Q_{bmij}} + \frac{R_{ij}}{Q_{mij}} \right)$$

$$PFp = 1 + \sum_{i} \sum_{j} \left[ \frac{M_{ij}}{Q_{pij}} \right] / Q_{pij}$$

Where  $\lambda_{RC}$  is a hyperparameter used to distinguish between simulations with/without resource competition. When  $\lambda_{RC}$  is set to 0, there is no resource competition; if it is set to 1, resource competition is present.

For the two node DSA circuit (resource consumption of the controller assumed to be approximately zero), these become:

$$PFm = 1 + \lambda_{RC}CN \left[ \left( \frac{1}{Q_{b1A}} + \frac{R_{1A}}{Q_{1A}} \right) + \left( \frac{1}{Q_{b2A}} + \frac{R_{2A}}{Q_{2A}} \right) \right]$$

$$PFp = 1 + \lambda_{RC} \left( \frac{[M_{1A}]}{Q_{n1A}} + \frac{[M_{2A}]}{Q_{n2A}} \right)$$

The fraction of active promoters,  $R_{ij}$ , for each circuit node  $(R_{iA})$  in the iFFL is given below

$$R_{iA} = \frac{(k_{diA}[I_i][P_{iA}])^n}{(k_{diA}[I_i][P_{iA}])^n + (k_{iA})^n} \frac{1}{A_i}$$

 $R_{ij}$  for the controller nodes ( $R_{iB}$ ) are similar but without  $P_{ij}$  as the controller nodes do not partake in the circuit's feedback topology; rather, they exist on top of this topology for purposes of regulation.

$$R_{iB} = \frac{(k_{diB}[I_i])^n}{(k_{diB}I_i)^n + (k_{iB})^n}$$

Where  $I_i$ ,  $k_{dij}$ ,  $k_{ij}$ , and n denote the inducer for the *i*-th gene in the circuit, the association constant for the autoinducer protein binding reaction, the Michaelis-Menten constant for the inducer-protein complex and promoter binding reaction, and the Hill coefficient of the promoter binding reaction, respectively.  $A_i$  denotes repression mediated by the controller module, which is given generally by

$$A_i = 1 + S_c \left( \frac{X_i}{Q_{Xi}} + \lambda_{GC} \sum_{k} \frac{X_k}{Q_{Xk}} (1 - \delta_{ik}) \right)$$

Where  $S_c$ ,  $X_i$ , and  $Q_{Xi}$  represent the strength of the controller (concentration of dCas9 for the NCR controller, or a multiplier of the repressive moiety-promoter binding affinity for the local and global controllers), the fraction of dCas9 complexed with the *i*-th sgRNA, and the binding coefficient between the dCas9-sgRNA complex and the respective repressed promoter.  $1 - \delta_{ik}$  utilizes the Kronecker delta to add a contribution of terms other than the *i*-th term, as the *i*-th contribution is taken into account by  $\frac{X_i}{O_{Xi}}$ . The fraction of dCas9 complexes is given by:

$$X_{i} = \frac{{{{{\left[ {{M_{iB}}} \right]}}/{J_{i}}}}}{{1 + {{{\left[ {{M_{iB}}} \right]}/{J_{i}}} + {\lambda _{NCR}}\sum\nolimits_{k} {{{\left[ {{M_{iB}}} \right]}}/{J_{k}}\left( {1 - {\delta _{ik}}} \right)}}}$$

Where  $J_i$  represents the binding affinity between the output of the *i*-th circuit node ( $P_{iA}$ , the concentration of sgRNA, which is assumed to be roughly similar to the concentration of output protein) and dCas9. As this is a general model which models all three controller archetypes,  $\lambda_{GC}$  and  $\lambda_{NCR}$  are meta-parameters used to denote which controller archetype is being modeled, with  $\lambda_{GC}=1$  and  $\lambda_{NCR}=0$  denoting the global controller,  $\lambda_{GC}=0$  and  $\lambda_{NCR}=1$  denoting the NCR controller, and the local controller being denoted when both of these meta-parameters are

set to 0. The controller-specific forms of the generalized model applied to a two-node circuit are shown in Table 1 below:

	Local controller	Global controller	NCR Controller
$\lambda_{GC}$	0	1	0
$\lambda_{NCR}$	0	0	1
A <sub>1</sub>	$1 + S_c \left( \frac{X_1}{Q_{X1}} \right)$	$1 + S_c \left( \frac{X_1}{Q_{X1}} + \frac{X_2}{Q_{X2}} \right)$	$1 + S_c \left( \frac{X_1}{Q_{X1}} \right)$
<i>X</i> <sub>1</sub>	$\frac{{{{{[{M_{1B}}]}} / {J_1}}}}{{1 + {{{[{M_{1B}}]}} / {J_1}}}}$	$\frac{{{{{[{M_{1B}}]}} / {J_1}}}}{{1 + {{{[{M_{1B}}]}} / {J_1}}}}$	$\frac{[M_{1B}]_{J_1}}{1 + [M_{1B}]_{J_1} + [M_{2B}]_{J_2}}$

Table 1. Forms of the generalized equations for Switch 1 for the three controller archetypes applied to a two-node DSA circuit.

For generating the heatmaps for our steady-state analysis, the activation threshold of each single switch (i.e., the concentration of its inducer at which said switch is activated in the absence of the opposite inducer) was rescaled to 1 in all cases (Figures 1B-C, 2A-C, 4D&E) for fair comparison of WTA, single-activation, and coactivation basins across the I1-I2 planes for all scenarios.

#### **Controller Resource Consumption**

The base model does not include the resource consumption of the controller and simulates the dynamics for scenarios where the applied controller is resource neutral. That is,  $Q_{b1B}$ ,  $Q_{1B}$ ,  $Q_{b2B}$ , and  $Q_{2B}$  in the full resource competitive term below are assumed to be infinite (or the *CRC* parameter set to zero), making the last terms in the resource competitive equations negligible:

$$PFm = 1 + \lambda_{RC}CN \left[ \left( \frac{1}{Q_{b1A}} + \frac{R_{1A}}{Q_{1A}} \right) + \left( \frac{1}{Q_{b2A}} + \frac{R_{2A}}{Q_{2A}} \right) + CRC * \left[ \left( \frac{1}{Q_{b1B}} + \frac{R_{1B}}{Q_{1B}} \right) + \left( \frac{1}{Q_{b2B}} + \frac{R_{2B}}{Q_{2B}} \right) \right] \right]$$

$$PFp = 1 + \lambda_{RC}CN \left[ \frac{[M_{1A}]}{Q_{1A}} + \frac{[M_{2A}]}{Q_{2A}} + CRC * \left[ \frac{[M_{1B}]}{Q_{1B}} + \frac{[M_{2B}]}{Q_{2B}} \right] \right]$$

This is a biologically reasonable assumption; if the controller is guided by sgRNA or small particle production,  $Q_{b1B}$ ,  $Q_{1B}$ ,  $Q_{b2B}$ , and  $Q_{2B}$  >>  $Q_{b1A}$ ,  $Q_{1A}$ ,  $Q_{b2A}$ , and  $Q_{2A}$  (Q representing dissociation constants of gene expression resources such as RNAP or ribosomes) as binding times for the production of controller moieties will be much shorter than for circuit moieties;

consequently, the last four terms in the equation can be ignored. Increasing the *CRC* parameter is used to explore the effect of increasing controller resource consumption.

#### **Parameter Sensitivity Analysis**

A global sensitivity analysis was performed to examine the effects of parameter perturbation on circuit performance and dynamics. As the focus of this study is to understand controller performance, the sensitivity analysis was then focused on the kinetic parameters associated with the specific controller rather than the circuit or environment. For the global sensitivity analysis, all the kinetic parameters are randomly perturbed simultaneously in each simulation, using the Latin hypercube sampling approach to randomly select a parameter value between the 10<sup>-1</sup> to 10<sup>1</sup> range of each parameter's nominal value <sup>29</sup>. To explore smaller *J* values in Figure 2G, the range for *J* was set to 2-40 instead. For this global sensitivity analysis, the total number of evenly spaced intervals for sampling was set to 1,000, and a total of 1600 simulations were performed for each circuit.

In addition to the global sensitivity analysis, a local sensitivity analysis was also performed to investigate the relationship between the controller performance and perturbations in kinetic parameter  $J_i$ , which represents the dissociation constant between sgRNA and dcas9. For the local sensitivity analysis, a single parameter is perturbed to gain insight into the impact of that specific parameter on the circuit dynamics<sup>30</sup> In this study, the kinetic parameters J1 and J2 were perturbed by discretizing each parameter value into 40 evenly spaced intervals from 1 to 10. Following this sampling approach, we performed a total of 1,600 simulations for each circuit to cover a 40x40 plane in J1-J2 phase space. Similar to the global sensitivity analysis, the local sensitivity analysis is focused on the calculated coactivation region from each simulation.

#### **OrthoScore**

To assess the orthogonality of the resource-competitive and controller systems, we defined an orthogonality score obtained from the I1-I2 heatmap analysis of each system, which we coined OrthoScore. OrthoScore is calculated by assigning points in the renormalized I1-I2 heatmaps of both the system under study and the ideal no resource competition system to their respective activation basins (no activation, Switch 1 activation, Switch 2 activation, or coactivation basin). The fraction of points that fall in matching basins with points in the ideal case is reported as the OrthoScore. An OrthoScore of 1 indicates a perfectly orthogonal set of switches in the DSA circuit, and a lower OrthoScore indicates further deviation from the ideal, non-resource competitive scenario.

#### **ABBREVIATIONS**

CRC - Controller resource consumption

DSA - Dual self-activation

DSAC - Dual self-activation circuit

GC - Global Controller

iFFL - Incoherent feedforward loop

LC - Local controller

NCR - Negatively competitive regulator

No RC – No resource competition with no controller case

RC - Resource competition/ no controller case

CTS - Coactivation threshold shift

WTA - Winner-Take-All

#### **Author Contributions**

X.-J.T. conceived the study. X.-J.T., A.S., X. T., and J.R. designed the study. A.S. and J.R. performed simulation and computational analysis. A.S., J.R., X.-J.T. and X. T. wrote the manuscript. A.S., J.R., X.-J.T., and X. T. edited the manuscript.

#### **Notes**

The authors declare no competing financial interest.

### **Supporting Information**

NCR efficacy over the local controller in global sensitivity analyses with different symmetry settings; Distribution of global sensitivity analysis data for different symmetry settings; illustration of subscripts used in this work; Model Formulation; Parameter information including nominal set and range.

#### **ACKNOWLEDGEMENTS**

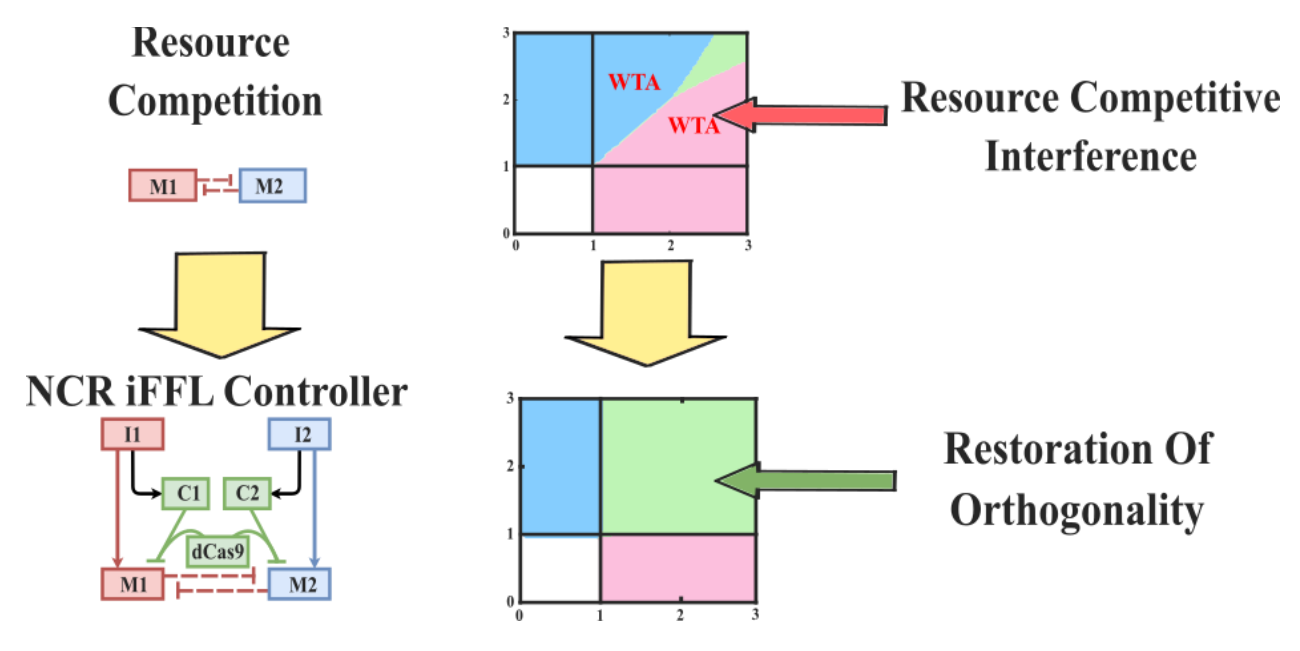
This project was supported NSF grants (2143229 to X-J.T.) and NIH grant (R35GM142896 to X-J.T.). A.S. was also supported by the Arizona State University Dean's Fellowship. X.T. and J.R. are supported by the startup fund provided by the Cain Department of Chemical Engineering at Louisiana State University.

#### **REFERENCES**

- (1) Cardinale, S., and Arkin, A. P. (2012, July) Contextualizing context for synthetic biology identifying causes of failure of synthetic biological systems. *Biotechnol J*.
- (2) del Vecchio, D. (2015, February 1) Modularity, context-dependence, and insulation in engineered biological circuits. *Trends Biotechnol*. Elsevier Ltd.
- (3) Boo, A., Ellis, T., and Stan, G. B. (2019, April 1) Host-aware synthetic biology. *Curr Opin Syst Biol*. Elsevier Ltd.
- (4) Grunberg, T. W., and del Vecchio, D. (2020, June 1) Modular Analysis and Design of Biological Circuits. *Curr Opin Biotechnol*. Elsevier Ltd.
- (5) Ilia, K., and Vecchio, D. del. (2022) Squaring a Circle: To What Extent Are Traditional Circuit Analogies Impeding Synthetic Biology? https://home.liebertpub.com/genbio 1, 150–155.
- (6) Klumpp, S., Zhang, Z., and Hwa, T. (2009) Growth Rate-Dependent Global Effects on Gene Expression in Bacteria. *Cell* 139, 1366–1375.
- (7) Borkowski, O., Ceroni, F., Stan, G. B., and Ellis, T. (2016, October 1) Overloaded and stressed: wholecell considerations for bacterial synthetic biology. *Curr Opin Microbiol*. Elsevier Ltd.
- (8) de Vos, D., Bruggeman, F. J., Westerhoff, H. v., and Bakker, B. M. (2011) How molecular competition influences fluxes in gene expression networks. *PLoS One 6*.
- (9) Qian, Y., Huang, H. H., Jiménez, J. I., and del Vecchio, D. (2017) Resource Competition Shapes the Response of Genetic Circuits. *ACS Synth Biol* 6, 1263–1272.
- (10) Zhang, R., Goetz, H., Melendez-Alvarez, J., Li, J., Ding, T., Wang, X., and Tian, X. J. (2021) Winner-takes-all resource competition redirects cascading cell fate transitions. *Nat Commun* 12, 1–9.
- (11) Goetz, H., Stone, A., Zhang, R., Lai, Y.-C., and Tian, X.-J. (2021) Double-edged role of resource competition in gene expression noise and control. *bioRxiv* 2021.10.29.466467.
- (12) Liu, C. C., Jewett, M. C., Chin, J. W., and Voigt, C. A. (2018, January 16) Toward an orthogonal central dogma. *Nat Chem Biol*. Nature Publishing Group.
- (13) Darlington, A. P. S., Kim, J., Jiménez, J. I., and Bates, D. G. (2018) Dynamic allocation of orthogonal ribosomes facilitates uncoupling of coexpressed genes. *Nat Commun 9*, 1–12.
- (14) Zhang, H., Pereira, B., Li, Z., Stephanopoulos, G., and Demain, A. L. (2015) Engineering Escherichia coli coculture systems for the production of biochemical products. *Proc Natl Acad Sci U S A 112*, 8266–8271.
- (15) Zhou, K., Qiao, K., Edgar, S., and Stephanopoulos, G. (2015) Distributing a metabolic pathway among a microbial consortium enhances production of natural products. *Nat Biotechnol 33*, 377–383.
- (16) Stone, A., Zhang, R., and Tian, X.-J. (2021) Coupling Shared and Tunable Negative Competition Against Winner-Take-All Resource Competition Via CRISPRi Moieties. *American Control Conference (Accepted)*.

- (17) Hamadeh, A., and del Vecchio, D. (2014) Mitigation of resource competition in synthetic genetic circuits through feedback regulation, in *Proceedings of the IEEE Conference on Decision and Control*, pp 3829–3834. Institute of Electrical and Electronics Engineers Inc.
- (18) Shopera, T., He, L., Oyetunde, T., Tang, Y. J., and Moon, T. S. (2017) Decoupling Resource-Coupled Gene Expression in Living Cells. *ACS Synth Biol* 6, 1596–1604.
- (19) Ceroni, F., Boo, A., Furini, S., Gorochowski, T. E., Borkowski, O., Ladak, Y. N., Awan, A. R., Gilbert, C., Stan, G. B., and Ellis, T. (2018) Burden-driven feedback control of gene expression. *Nat Methods* 15, 387–393.
- (20) Huang, H. H., Qian, Y., and del Vecchio, D. (2018) A quasi-integral controller for adaptation of genetic modules to variable ribosome demand. *Nat Commun 9*, 1–12.
- (21) Bleris, L., Xie, Z., Glass, D., Adadey, A., Sontag, E., and Benenson, Y. (2011) Synthetic incoherent feedforward circuits show adaptation to the amount of their genetic template. *Mol Syst Biol 7*, 519.
- (22) Ma, W., Trusina, A., El-Samad, H., Lim, W. A., and Tang, C. (2009) Defining Network Topologies that Can Achieve Biochemical Adaptation. *Cell* 138, 760–773.
- (23) Kaplan, S., Bren, A., Dekel, E., and Alon, U. (2008) The incoherent feedforward loop can generate non-monotonic input functions for genes. *Mol Syst Biol 4*, 203.
- (24) Westbrook, A., Tang, X., Marshall, R., Maxwell, C. S., Chappell, J., Agrawal, D. K., Dunlop, M. J., Noireaux, V., Beisel, C. L., Lucks, J., and Franco, E. (2019) Distinct timescales of RNA regulators enable the construction of a genetic pulse generator. *Biotechnol Bioeng* 116, 1139–1151.
- (25) McBride, C. D., Grunberg, T. W., and del Vecchio, D. (2021) Design of genetic circuits that are robust to resource competition. *Curr Opin Syst Biol* 28, 100357.
- (26) Frei, T., Cella, F., Tedeschi, F., Gutiérrez, J., Stan, G. B., Khammash, M., and Siciliano, V. (2020) Characterization and mitigation of gene expression burden in mammalian cells. *Nature Communications* 2020 11:1 11, 1–14.
- (27) Barajas, C., Gibson, J., Sandoval, L., and Vecchio, D. del. A burden-free gene overexpression system.
- (28) Jones, R. D., Qian, Y., Siciliano, V., DiAndreth, B., Huh, J., Weiss, R., and del Vecchio, D. (2020) An endoribonuclease-based feedforward controller for decoupling resource-limited genetic modules in mammalian cells. *Nat Commun* 11.
- (29) Helton, J. C., and Davis, F. J. (2003) Latin hypercube sampling and the propagation of uncertainty in analyses of complex systems. *Reliab Eng Syst Saf 81*, 23–69.
- (30) Morio, J. (2011) Global and local sensitivity analysis methods for a physical system. *Eur J Phys 32*, 1577.

**Figures** 



**Abstract Graphic.** 

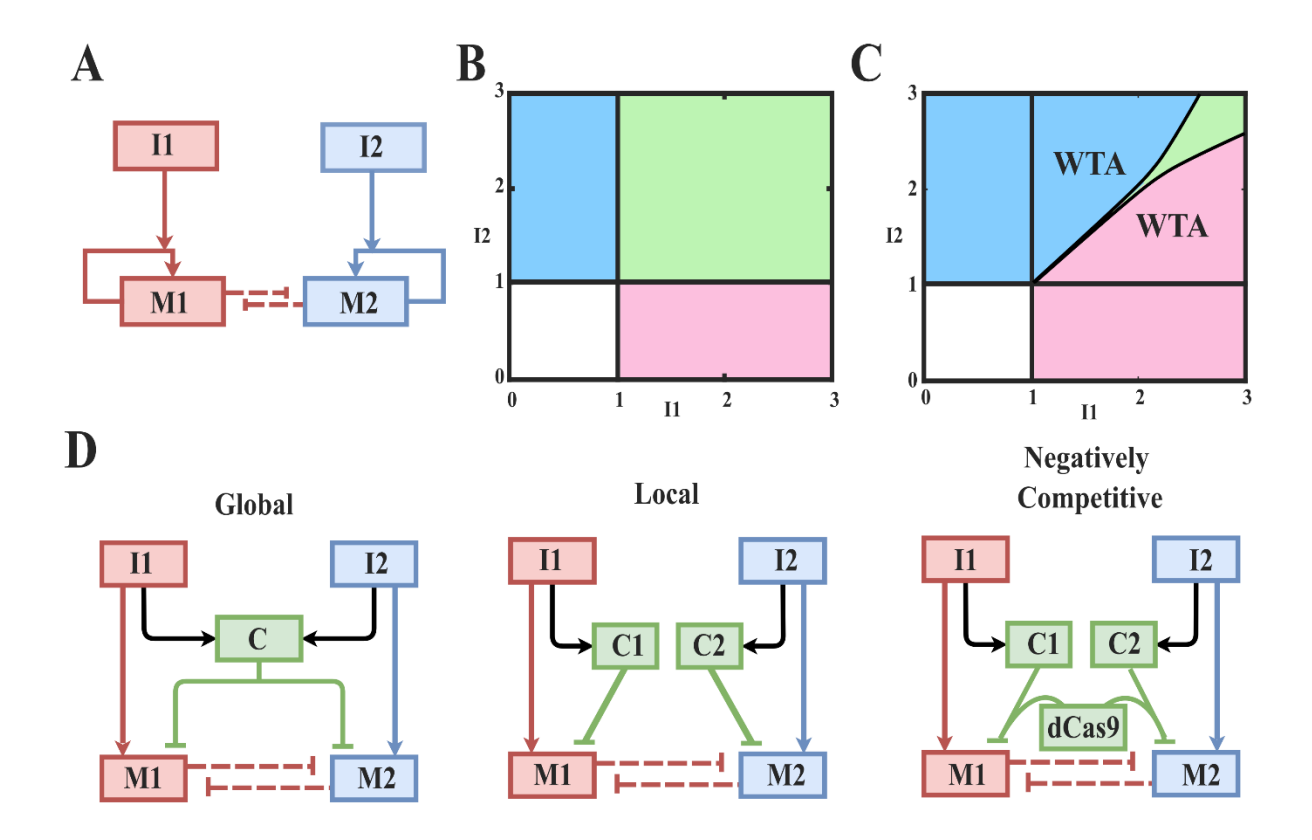


Figure 1. Effect of resource competition on the dual self-activation switch circuit and resource competitive controller topologies. A) Topology of the dual self-activation (DSA) circuit, where two unlinked self-activation switches (with inducers I1 and I2 respectively) interact with each other due to resource competition. B-C) Steady-state heatmaps across the inducer I1-I2 plane for the ideal DSA circuit without the presence of resource competition (B) and with resource competition (C). Magenta, blue, green, and white regions delineate the switch 1 activation, switch 2 activation, coactivation, and no activation basins respectively, whereas the black lines denote the basin thresholds of the ideal, non-resource competitive case. D) Topology of the 3 types of resource competitive controllers, mediated via incoherent feedforward network motifs. In the case of NCR, C1 and C2 represent repressive sgRNA moieties that can only mediate repression after forming a repressive complex with a dCas9.

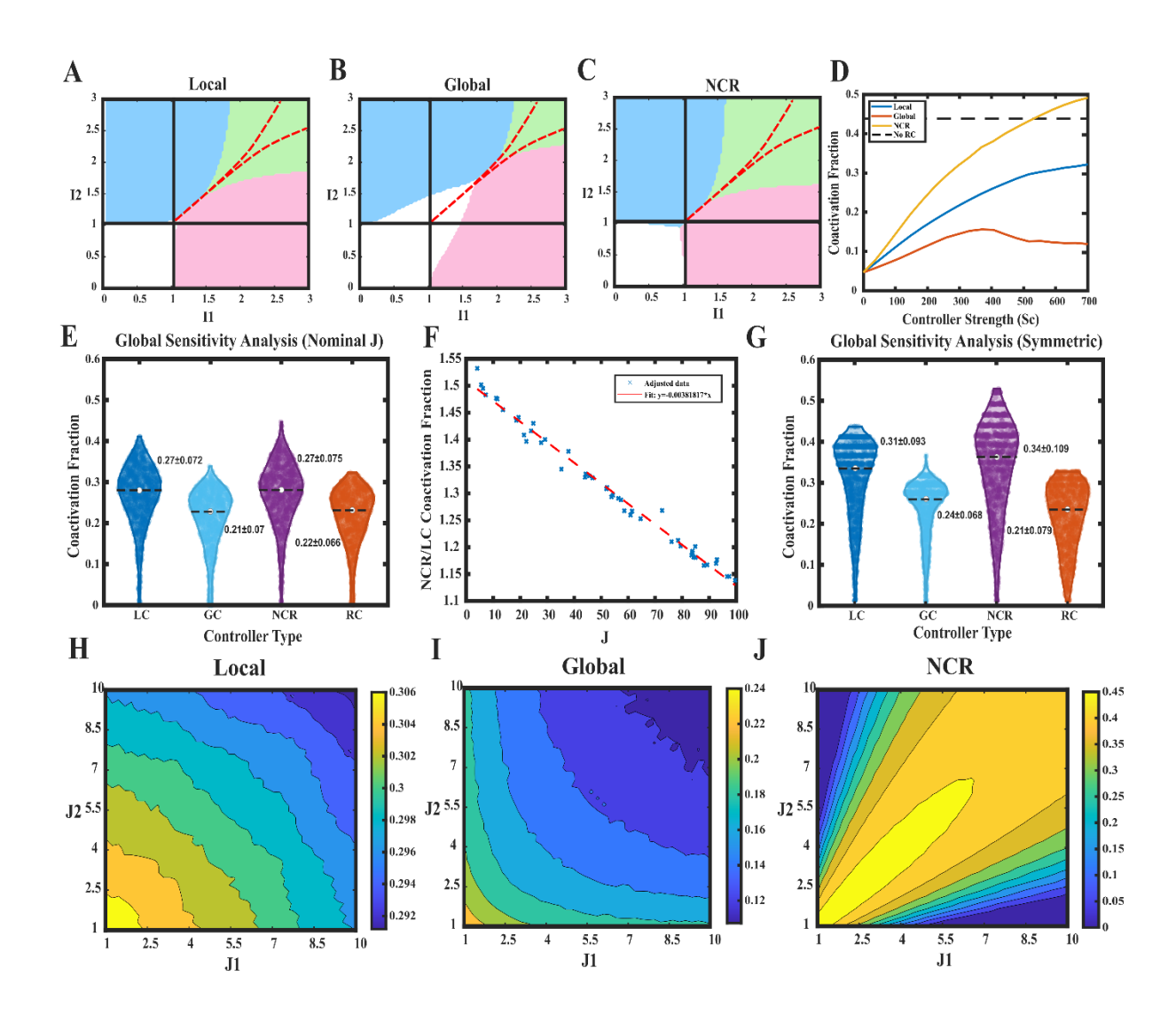


Figure 2. Effect of the resource competitive controllers on winner-take-all resource competition. A-C) Steady-state heatmaps of the local (LC), global (GC), and NCR controller types. Coactivation basins are significantly expanded compared to the resource competitive system alone (Figure 1C). Red dashed lines correspond to the basin boundaries in the no controller case. **D)** Fraction of parameter space taken up by the coactivation basin for the controller systems vs controller strength (Sc), which is characterized by the concentration of repressive dCas9 present in the cell for the NCR controller or as a multiplier on the repressive complex-promoter binding affinity for the local and global controllers. 'No RC' here refers to the scenario with no resource competition or controller applied. **E)** Global parameter sensitivity analysis for each controller type compared to the no controller case with resource competition (RC) with the nominal value of J = 50. **F)** Local sensitivity analysis showing the ratio between NCR and LC coactivation fractions over J. **G)** Global parameter sensitivity analysis with reduced J (ranging from 2 to 40) and full system symmetry constraint applied. H-J) Local parameter sensitivity analysis displaying coactivation fraction for each controller type over the J1-J2 plane, demonstrating distinct controller responses to system asymmetry.

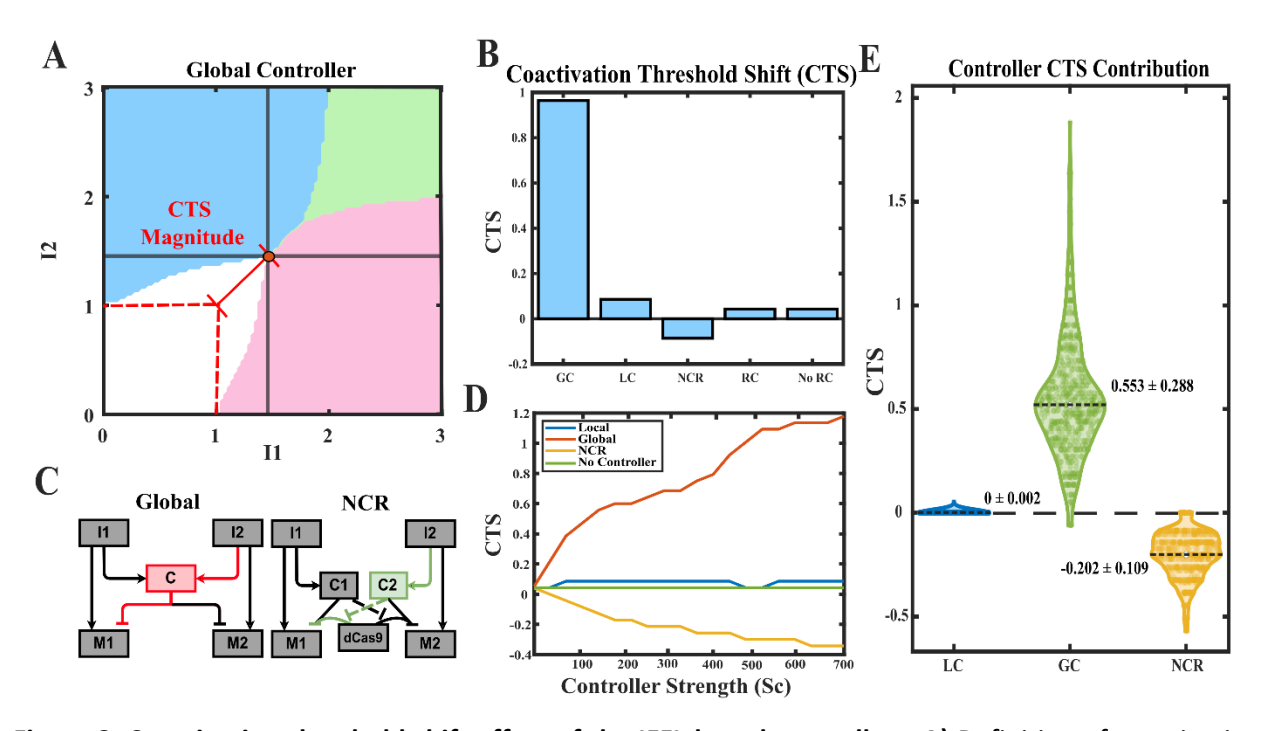


Figure 3. Coactivation threshold shift effect of the IFFL-based controllers. A) Definition of coactivation threshold shift (CTS) phenomenon. CTS is characterized by the distance between the position of the dual-activation point (red dot) in the ideal, non-resource competitive case (1,1) and the dual-activation point of the system with controller applied. B) Magnitude of the CTSeffect of different controllers. CTS here was gathered from the local, global, and NCR heatmaps in Figures 2A-C and the base no-controller systems with (RC) or without (no RC) resource competition from Figures 1B&C. Due to the cross-lateral effects, the global and NCR controllers display significant positive and negative CTS effects respectively C) Biochemical mode of action for CTS phenomena. The left diagram shows the cross-lateral inhibition present in the global controller construct responsible for its characteristic positive CTS, whereas the right shows the cross-lateral activation present in the NCR controller responsible for its negative coactivation shift. Introduction of I2 in the NCR system results in the portion of the controller targeting M2 to pull dCas9 away from M1, thus suppressing the inhibition on M1, and resulting in a net activatory effect. The dashed lines are for illustration purposes and are not links present in the circuit topology. D) CTS trends across different controller strengths. E) Global parameter sensitivity analysis demonstrates that these trends in controller contribution to the CTS are robust across the biologically relevant parameter space, with GC adding a distinct positive CTS contribution, NCR a negative one, and LC a relatively neutral one.

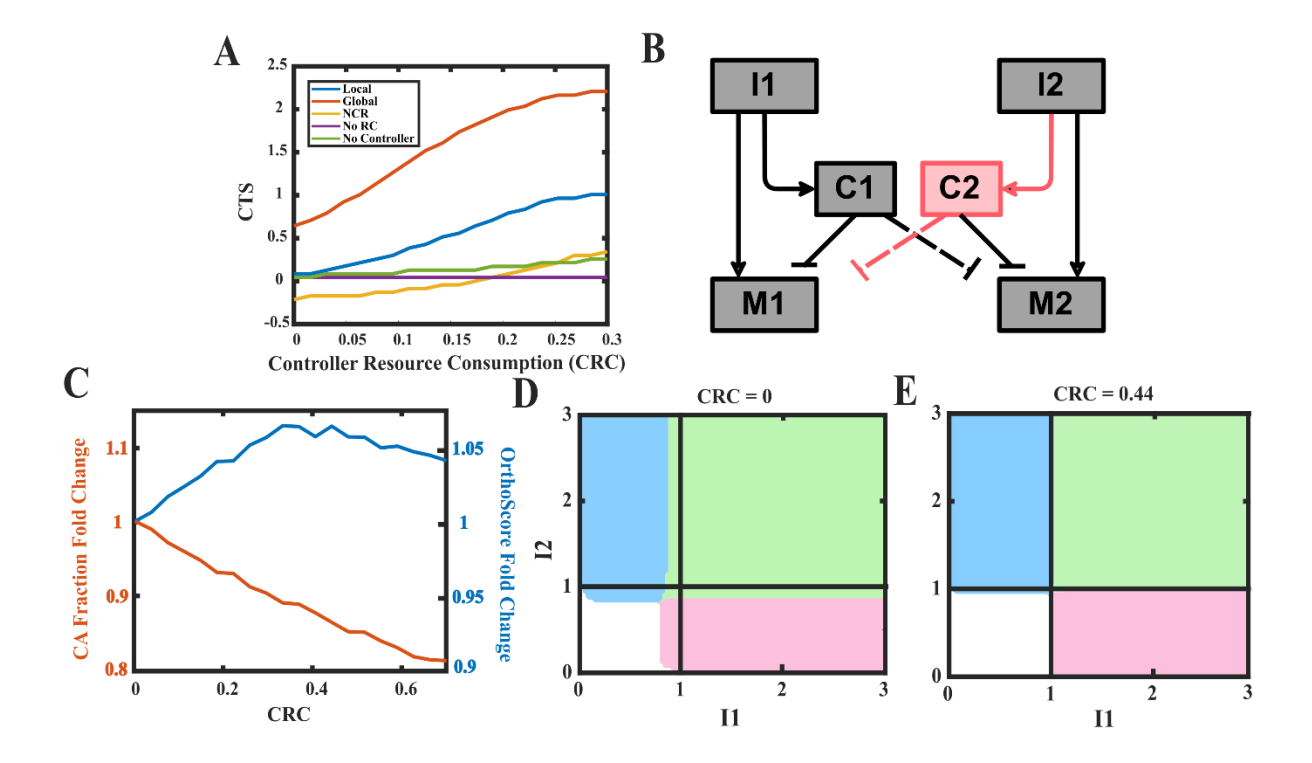


Figure 4. Effect of controller resource competition on coactivation threshold shift and switch orthogonality. A) Effect of controller resource competition on CTS. Controller resource competition adds positive contribution to CTS on top of the CTS already imbued to the system by the controller. The added positive magnitude increases as the resource consumption of the controller nodes increases. B) Biochemical mechanism for the consistent positive CTS of controller resource consumption; consumption of resources by the controller inhibits the contralateral node independent of controller type. C) Effect of controller resource consumption on the coactivation fraction and orthogonality of the NCR controller. The left y-axis corresponds to the coactivation fraction graph, while the right y-axis corresponds to the OrthoScore graph. As controller resource consumption increases, the positive CTS from the controller resource consumption mitigates the natural negative CTS of the NCR controller. This sacrifices coactivation fraction for orthogonality. D-E) Depictions of the NCR controller without controller resource consumption (D) and with the level of controller resource consumption optimal for system orthogonality (E).